JOURNAL OF MATERIALS SCIENCE 22 (1987) 1469–1476

Solidification microstructures in rapidly solidified, gas atomized aluminium–lithium alloy powders

G. VON BRADSKY, R. A. RICKS*
Department of Materials Science and Engineering, University of Surrey, Guildford, Surrey GU2 5XH, UK

The examination of the solidification behaviour and resultant microstructures in an Al–Li–Cu–Mg–Zr alloy processed by high-pressure inert gas atomization is reported. Using analytical transmission electron microscopy some quantification of the segregation behaviour is possible which allows the comparison with a simple solute redistribution model (Scheil analysis). It is shown that for powder sizes likely to be of commercial interest (10 to 20 μm), cellular solidification structures are to be expected on atomization, and methods of utilizing such structures are discussed.

1. Introduction

The development of low density, high modulus aluminium-base alloys for aerospace application has concentrated to date on a variety of aluminium–lithium alloys, often containing other elemental additions to improve further the mechanical properties. For many applications the reduction in component weight may be the prime consideration, for which purpose high lithium additions would be desirable. Using conventional ingot technology processing routes, lithium additions in excess of approximately 3 wt % can lead to problems associated with chemical segregation and ingot cracking. Even if such casting problems could be overcome, an upper limit to lithium additions would still exist owing to the inability to take into solution more than ≈ 4 wt % Li additions in the α-aluminium matrix. Such solution heat treatments are necessary with case alloys to allow both homogenization of the ingot and the subsequent precipitation of Al_3Li (δ') which imparts much of the mechanical strength to the component.

In addition, the development of alloys which rely upon precipitation hardening to develop adequate service properties often presents problems when dynamic property improvements are sought. The coherent δ' formed in lithium-containing alloys effectively localizes slip on to few active slip planes during deformation allowing the development of stress concentrations at grain boundaries. This can lead to poor fracture and fatigue resistance and hence the addition of other precipitation-hardening elements (e.g. copper, magnesium) may help by the generation of precipitate morphologies and dispersions which hinder the localization of slip and improve alloy toughness (e.g. [1, 2]).

The benefits of rapid solidification processing (RSP) for aluminium alloys are now well documented and many alloy development programmes are currently seeking to utilize this processing route. Advantages over ingot technology include the total removal of macrosegregation and a reduction in the scale of microsegregation leading to an overall refinement of the microstructure. In addition, with a suitable choice of alloy composition, solid solution extension is also possible and has been reported in a number of alloys. In view of the aforementioned processing limitations applicable to aluminium alloys containing high lithium additions using conventional techniques it is clear that RSP could well be beneficial for the future development of low-density materials.

Until recently one of the major limitations of RSP has been the low productivity rates and the production of rapidly solidified material in a form suitable for subsequent processing. Since all RSP techniques rely upon the minimization of a least one dimension of the molten material to maximize heat extraction rates, the final processing of such material must always involve some compaction stage. Thus some microstructural alteration with possible concomitant property modifications are to be expected. The process of twin fluid gas atomization using inert gas at high pressure has been shown to be capable of the bulk production of powdered material at heat extraction rates comparable to many processes associated with RSP [3, 4]. Solidification microstructures identical to those obtained by melt spinning and splat quenching may be produced by powder metallurgical routes provided the particle diameter is low. However, owing to the limitation of heat extraction solely by the atomizing gas, heat transfer coefficients during atomization only approach those associated with other RSP techniques for droplet sizes below ~ 10 mm [3]. It is not likely that such ultrafine powders will be of commercial significance in the near future owing to the safety

Present address: Alcan International Ltd, Banbury Laboratories, Southam Road, Banbury, Oxfordshire OX16 7SP, UK.

0022–2461/87 $03.00 + .12

and handling problems caused by such finely divided material.

The purpose of this work is to assess the solidification microstructures and possible benefits pertaining to the power sizes likely to be of commercial interest (10 to 30 mm) in an Al–Li alloy. Analytical transmission electron microscopy has been used extensively to characterize the microstructures formed and the solute segregation has been related to the interfacial conditions prevalent during solidification using a simple solute redistribution model. It is shown that equilibrium partitioning occurs at the solidification front for all but the finest particle sizes, leading to a fine cellular microstructure. This solidification behaviour is compared with that observed in other alloys produced by gas atomization, and methods of exploiting such microstructures for the attainment of improved mechanical properties will be discussed.

2. Experimental procedure

For the purposes of this study a conventional alloy composition was chosen, having a nominal composition based on Al–2.5% Li–1.2% Cu–0.6% Mg–0.12% Zr. The alloy was produced in a powdered form using the twin fluid inert-gas atomizer at the University of Surrey. The details of this equipment and atomization procedure may be found elsewhere and will not be considered here [5, 6]. It is worth noting that the design of atomizing die used for the present investigation was not intended to generate ultrasonic pressure modulations or shock waves as reportedly employed by other workers [7]. Gas pressures were limited to generate exit gas velocities in the transonic regime: no provision is yet available for the production of supersonic gas jet velocities.

The powders produced were prepared for examination by transmission electron microscopy by one of two methods. Very fine powders ($< 5\,\mu m$) were best prepared by embedding in a suitable resin and using ultramicrotomy to cut thin slices (≈ 100 nm thick) of the resultant composite solid. This method rapidly generates a large number of sections suitable for examination and although some obvious deformation is induced into the microstructure, phase identification and chemical microanalysis is still possible. For larger particles, however, the residual stresses incurred by the cutting process cause the sections to curl up and thus be unsuited to examination in the transmission microscope. Other problems involving specimen stability in the electron beam (especially when attempting analysis) meant that alternative means of specimen preparation were required, involving the incorporation of the powders in a nickel matrix using plating techniques. The embedding process consists of the simultaneous gravity deposition of powder and electrodeposition of nickel on to a horizontal, polished stainless steel cathode from a suspension of the specimen powder in a nickel sulphamate bath. By a suitable choice of powder concentration it was possible to firmly embed the particles in the developing nickel matrix. Optimum conditions were obtained with the bath at 50 to 60° C and a current density of 50 $\mu A\,cm^2$ using pure nickel anodes. Foils of approximately 100 to 150 μm thickness could be obtained in 2 to 3 h. Discs, 3 mm diameter, were then punched from the plated foils and mechanically polished to $\approx 60\,\mu m$ prior to final thinning to perforation using ion-beam milling. All electron microscopy was performed on a Philips EM400T fitted with both windowless energy dispersive spectrometry equipment and an electron energy loss spectrometer.

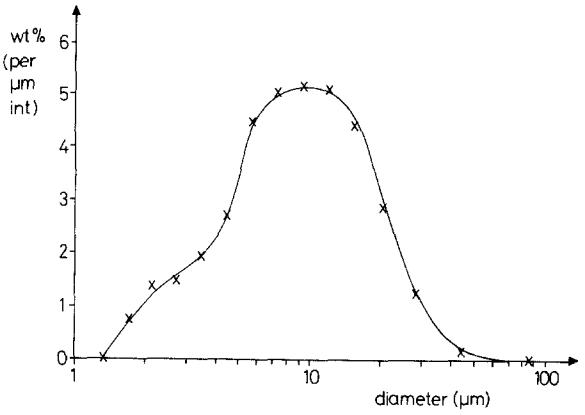

Figure 1 Particle size distribution obtained from a sample of Al–2.5Li–1.2 Cu–0.6 Mg–0.12 Zr as-atomized powder as used in this investigation. $d_{mn} = 1.57\,\mu m$, $d_{med} = 14\,\mu m$.

3. Results

The details of the heat and fluid flow phenomena pertinent to atomization have been considered recently by Clyne *et al.* [3, 6]. For gas exit velocities in the range 10 to 100 m sec^{-1} using pure helium as an atomizing gas, heat transfer coefficients can be shown to be a relatively sensitive function of particle size. For particles $\approx 10\,\mu m$ diameter, values of the heat transfer coefficent for these atomizing conditions are expected to be in the range 5×10^5 to $10^5\,W\,m^{-2}\,K^{-1}$. Characterization of the resultant atomized powder was performed using laser granulometry and this showed that the sample had a median diameter of ≈ 4 mm with a size distribution as illustrated in Fig. 1. Note that the vast majority of particles produced were below 40 μm.

Powder morphology was examined by scanning electron microscopy and Fig. 2 shows a typical sample. Particles were spherical, as expected for atomized

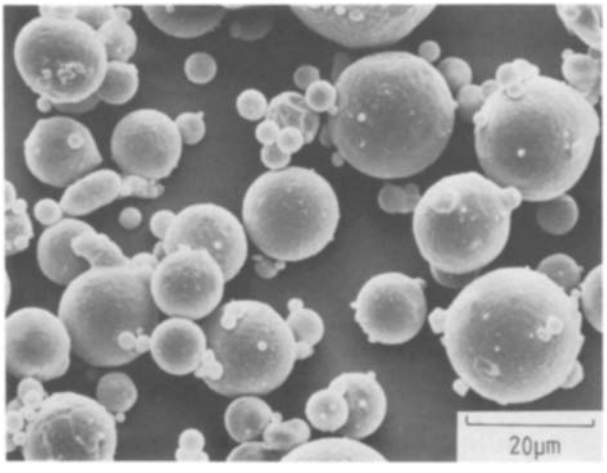

Figure 2 Scanning electron micrograph showing powder morphology.

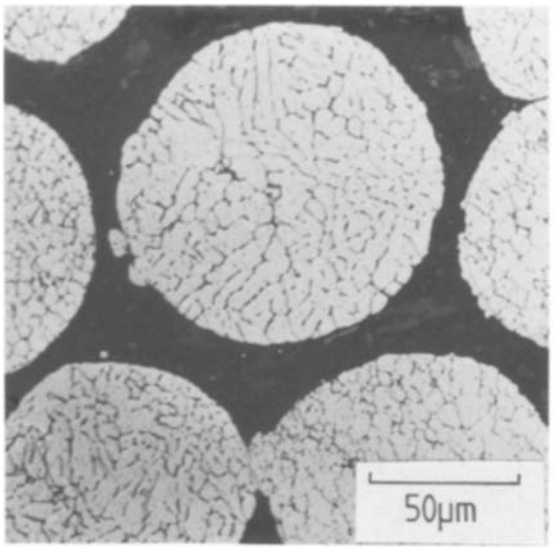

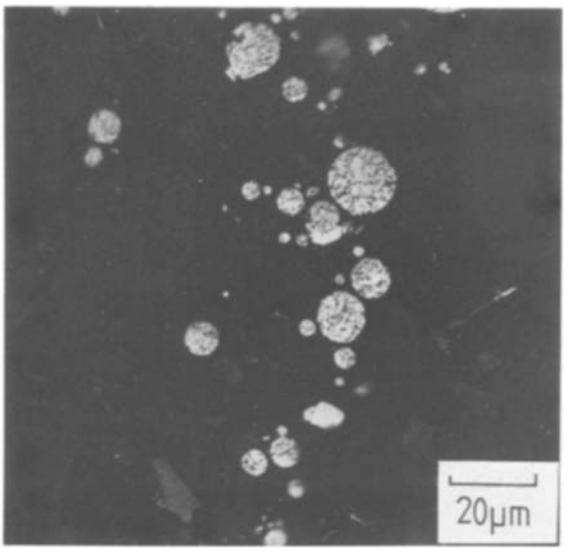

Figure 3 Light micrograph showing cellular solidification structure associated with the majority of powder sizes.

powder produced under non-oxidizing conditions, indicating that solidification had taken place during flight. A significant satellite population was observed (Fig. 2) caused by the collision of small, solidified droplets with larger, still molten material (and causing premature nucleation). For the purposes of this study such satellites proved invaluable since it is unlikely that such fine powder could be collected by the present design of cyclone used.

Examination of the microstructure of the powders using light microscopy revealed that the majority of particles exhibited a cellular microstructure (Fig. 3), the scale of which depends on the overall particle size. Transmission electron microscopy revealed that such solidification structures were present in particles down to $\approx 5\,\mu m$ (Fig. 4) indicating that solute rejection had occurred during solidification leading to the development of constitutional undercooling effects, which would allow the destabilization of a planar interface, thus generating a cellular microstructure. The refinement of the microstructure as a function of particle size (and hence heat extraction rate) is obvious from these micrographs and is quantified in Fig. 5.

Particles below $\approx 2\,\mu m$ section diameter displayed featureless microstructures of single-phase α-aluminium (Fig. 6). Such microstructures result from the extremely high heat extraction rates associated with these particle sizes which leads to rapid crystal growth velocities. This heat extraction, combined with a high nucleation undercooling (see [3]) effectively avoids recalescence effects which tend to reduce the solidification front velocity by raising the interfacial temperature. By maintaining a high growth undercooling the velocity of the interface is such that solute trapping takes place due to the inability of the solute atoms to diffuse ahead of the interface. The resultant microstructure is thus highly supersaturated and of single phase. Interesting combinations of partially cellular, partially featureless particle microstructures may be produced in particles between 2 and $5\,\mu m$ diameter caused by the variation in interfacial velocity generated by the evolution of latent heat during solidification. These microstructures have been described in more detail by Ricks [8] and will not be considered further here.

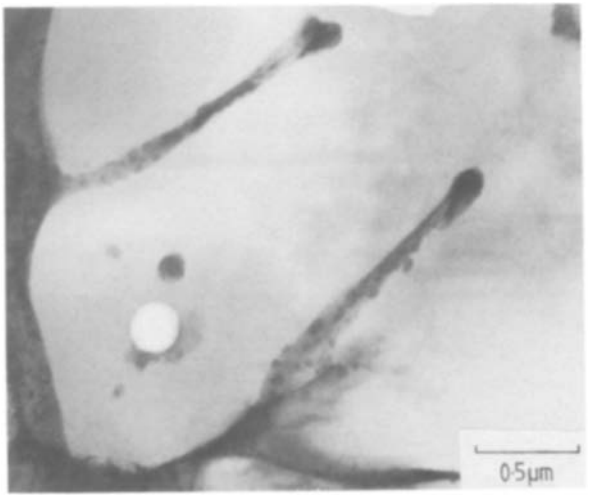

Figure 4 Transmission electron micrograph showing presence of cellular structure in powder sections down to $\approx 5\,\mu m$.

Analysis of the chemical segregation behaviour during solidification was performed using energy dispersive spectrometry (EDS) (heavy elements, i.e. $Z > 13$) and electron energy loss spectrometry (EELS) for lithium detection. EDS analysis revealed significant heavy-element segregation to the intercellular regions as shown in Fig. 7 with substantial variations in detected quantities obtained as a function of probe position within the intercellular region

TABLE I Results of EDS analysis

	Al (wt %)	Cu (wt %)	Mg (wt %)	Fe (wt %)
Intercellular regions	72.6	21.5	3.9	1.9
	85.6	10.4	2.5	1.4
	76.9	17.3	3.6	2.0
	94.9	3.6	1.1	0.3
	91.3	5.9	2.0	0.4
	80.0	13.2	2.9	4.2
	76.9	16.4	3.7	3.0
Cell interiors	99.5	0.4	0.1	–
Sub 2 μm particles	97.9	1.3	0.5	0.2

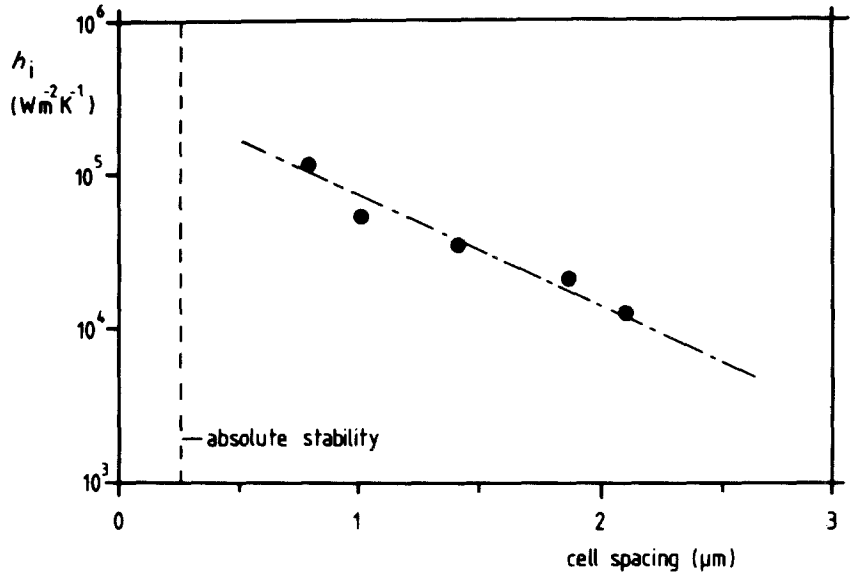

Figure 5 Plot of cell spacing as a function of heat transfer coefficient.

(see Section 4). Variations in composition across the cellular structure were difficult to monitor owing to the low levels of solute present but some data were obtained and these are presented in Fig. 8 as a composition profile up to a cell boundary (see Section 4). Microanalysis of the small, structureless particle sections was undertaken to determine the overall composition of the alloy. These results are given in Table I.

Of the techniques currently available for the detection of light elements only EELS has the ability to obtain information with sufficiently high spatial resolution and was consequently used in this investigation. Analysis may be performed with lower spatial resolution using the technique of laser-induced ion mass analysis (LIMA) (spatial resolution $\approx 1\,\mu m$) and this has been employed in the past to check the solute levels in the alloy before and after atomization [9] to verify that little or no solute loss occurred during processing. One major problem in the use of EELS to detect lithium in an aluminium matrix is due to the presence of the plasmon peaks associated with the aluminium, the third of which usually masks any lithium edge present. To overcome this problem the specimen thickness must be reduced to avoid producing any signal due to a third plasmon peak; this implies a specimen thickness of less than $\approx 40\,nm$. Although ultramicrotomy of such thin sections was not possible, certain regions of the foils produced by ion-beam milling did meet this thickness criterion and consequently successful detection of lithium was possible.

Fig. 9 presents EELS data obtained from an intercellular region (Fig. 9a) and from the centre of a cell interior (Fig. 9b). These data indicate that lithium is only present in detectable quantities in the intercellular regions. Detection limits for lithium in aluminium have been considered previously [10] and concentrations greater than $\approx 2.7\,wt\,\%$ are required for detection. Thus the detection of lithium in the intercellular regions indicates a level of lithium greater than this, and quantification of these data has been performed to provide the results presented in Table II. Quantification of the EELS data was undertaken following the method outlined by Chan and Williams [10]. By implication, the centre of the cells would be considerably reduced in lithium content and clearly no detection would be expected. These results, therefore, show that partitioning of lithium, as well as the heavier elements, takes place during solidification.

Further evidence to indicate that equilibrium partitioning of lithium has taken place at the solidification interface is presented in Fig. 10. As lithium is rejected by the solid (partition coefficient = ≈ 0.5) the concentration of lithium in the liquid would increase. For a given constant partition coefficient and assuming complete mixing in the liquid with no back diffusion in

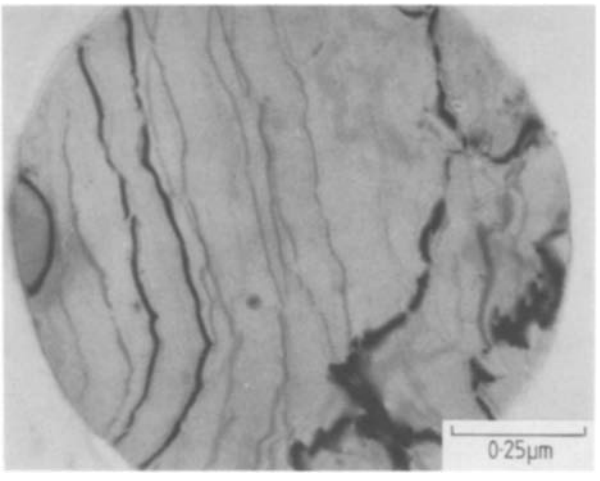

Figure 6 Transmission electron micrograph image showing segregation free microstructure associated with ultrafine droplet ($< 2\,\mu m$ diameter).

TABLE II Results of EELS analysis

	Al/Li ratio	
δ' in bulk alloy	5.05 : 1	
	4.42 : 1	mean = 5.03 : 1
	5.63 : 1	= 16.5 at % Li
Intercellular region in powders	3.73 : 1	
	2.38 : 1	mean = 2.705 : 1
	2.56 : 1	= 27.0 at % Li
	2.15 : 1	

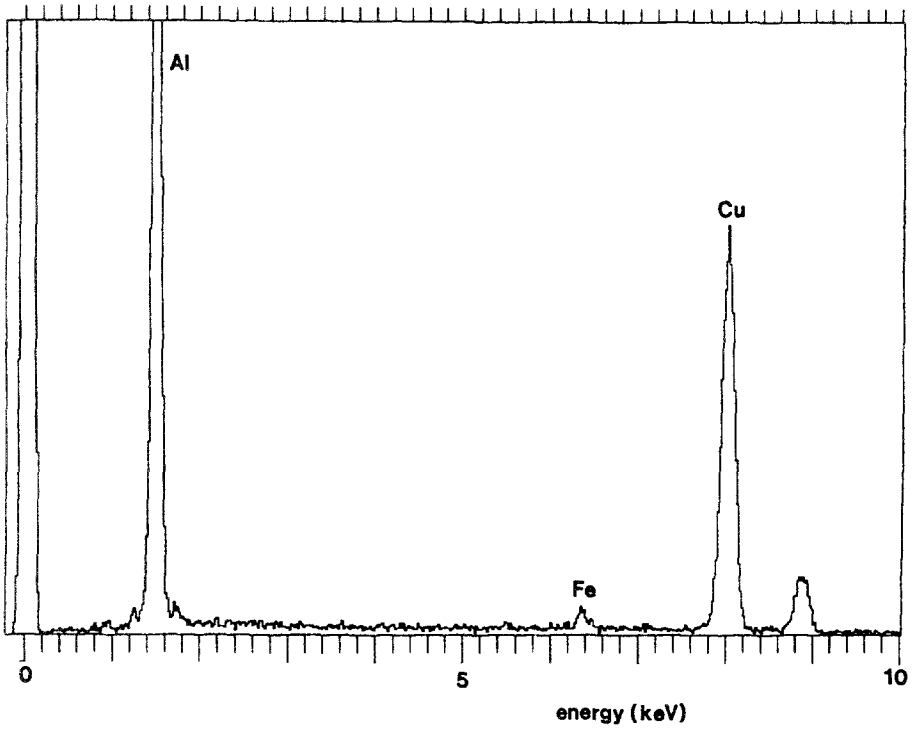

Figure 7 EDS spectrum from an intercellular region showing segregation of copper and iron.

the solid, the level of lithium present in the solid would increase towards the cell boundary. Above ≈ 1.5 wt % lithium the precipitation of the metastable δ' (A_3Li) phase would be expected and Fig. 8 shows the presence of this phase in regions adjacent to the cell boundaries indicating local lithium concentrations in excess of this. (See also Section 4.)

4. Discussion

In view of the safety and handling limitations imposed by ultrafine (i.e. 10 μm diameter) particles it would appear that, for alloy systems exhibiting partition coefficients less than one, cellular solidification microstructures are to be expected in the size range of particles likely to be of most immediate interest. Similar studies with other eutectic alloys show the same result and the extension of solid solution ranges would not appear to be feasible given the inability to improve the value of the heat transfer coefficient associated with these particle sizes.

It is of interest to compare the solute levels detected experimentally across the cellular microstructure with those predicted by a simple solute distribution model. For the likely conditions of interfacial velocity and

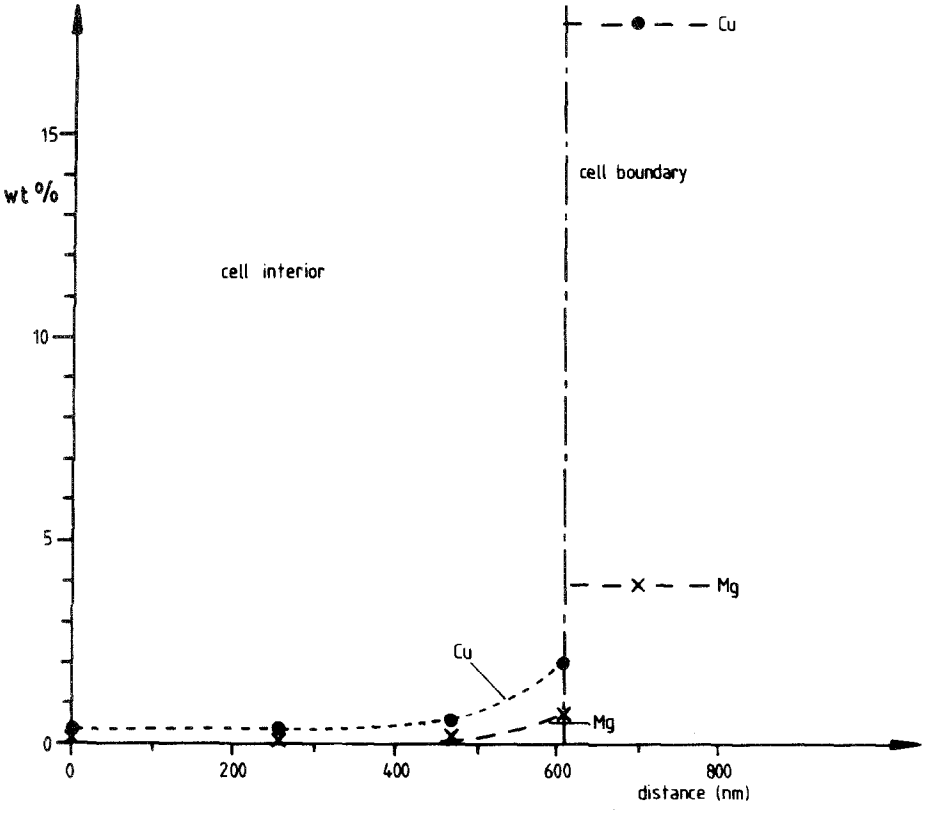

Figure 8 Experimentally determined concentration profile across a cell.

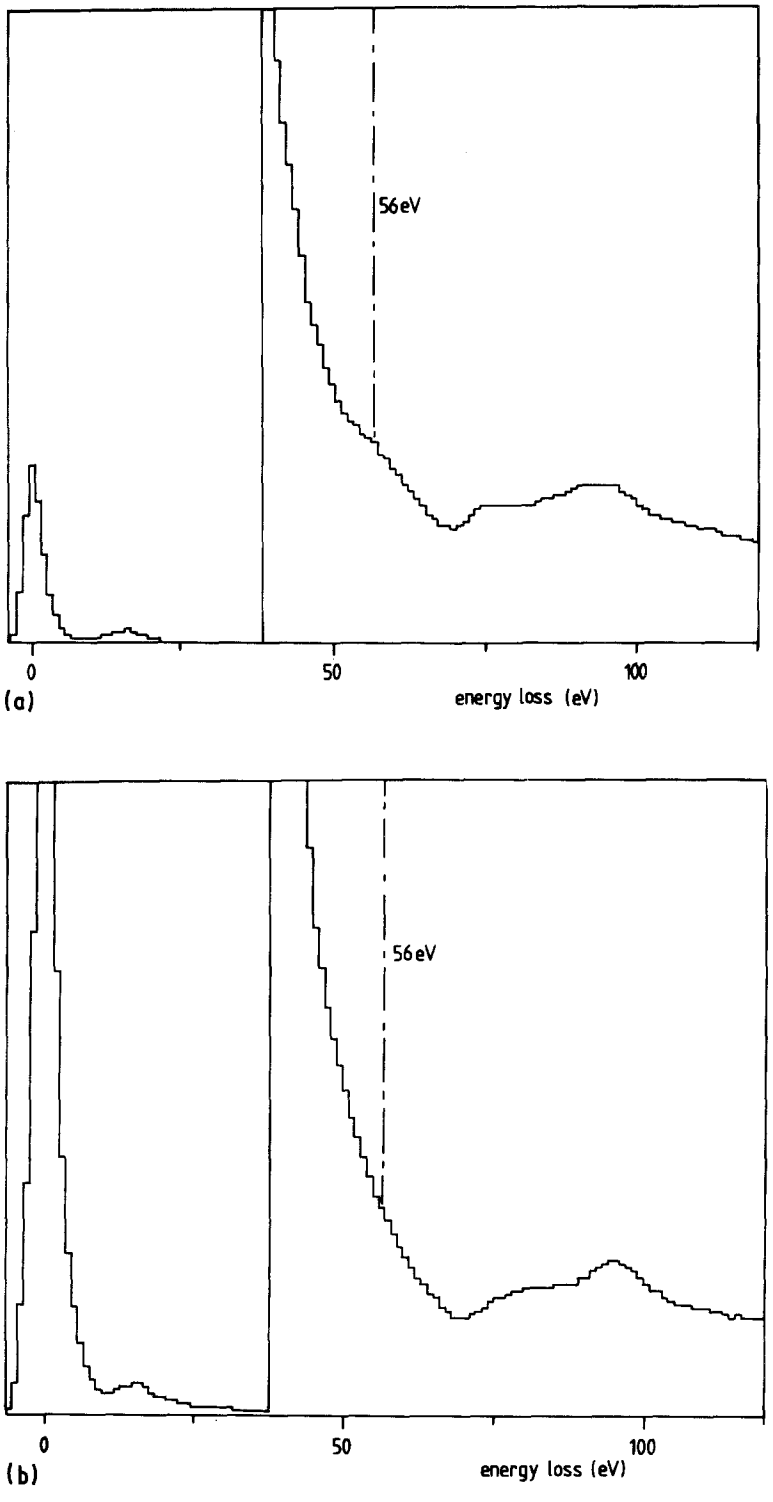

Figure 9 EELS spectra obtained from (a) an intercellular region and (b) cell centre showing presence of detectable quantities of lithium in the intercellular regions.

temperature gradient, the lateral growth of each cellular protrusion on the growth interface will most probably correspond to those pertaining to the Scheil analysis (e.g. [11]). Given this premise, predicted solute levels as a function of volume fraction of solid may be calculated for a given value of the partition coefficient. Such data are presented in Fig. 11 for the relevant solute elements, assuming equilibrium binary partition coefficients; lateral growth of the cells is assumed to cease when the lithium level in the liquid (the major alloying element present) reaches the eutectic level. Comparison of these predictions with the data presented in Fig. 8 show good agreement and the general indication is that equilibrium partitioning of solute is maintained at the solidification interface despite the high heat extraction rates experienced. Consideration of the appropriate isothermal section of the Al–Li–Cu ternary phase diagram indicate that the final liquid to solidify would do so to form a combination of δ (Al–Li) and τ_1 (and possibly τ_2) intermetallic phases (Fig. 12). This would then explain the variation in composition detected in the intercellular region as a function of probe position as reported in Section 3.

It is important, in view of these results, to consider exactly how best to utilize the solidification microstructures associated with atomization. Clearly interfacial velocities concomitant with complete solute trapping are only experienced with extremely fine powder particles, and in view of the large dependence of heat transfer coefficient on droplet size, it would

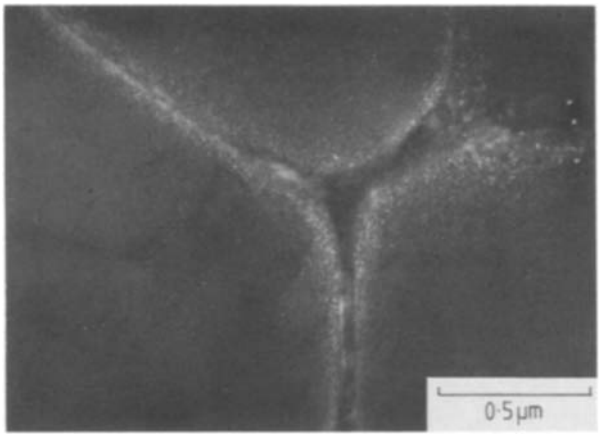

Figure 10 Centred dark-field transmission electron micrograph using (0 1 1) δ' reflection showing precipitation adjacent to cell boundary from lithium enriched regions of the aluminium cell matrix.

seem unlikely that enhanced solid solubilities are to be expected from this processing route. Alloy development programmes are already underway to achieve such microstructures given the limitations on heat transfer, but even the most optimistic considerations of variability of partition coefficient with interfacial velocity would indicate that sub 5 μm particles will be necessary. Thus cellular solidification microstructures are to be expected and many recent data confirm this (e.g. [12, 13]).

Recent work concerning the consolidation of powders displaying cellular solidification microstructures using extrusion-related techniques (e.g. CONFORM) indicate that break-up of the cells into a sub-grain structure of similar dimensions takes place, and this may be stabilized by the intermetallics which originate in the intercellular regions. This microstructural development under the intense shear stresses associated with such consolidation techniques is not unexpected, but what is more surprising is the mechanical strength and ductility, and thermal stability, displayed by such material (e.g. [14]). Clearly there is much scope for the development of alloys with more stable intermetallics to improve the high-temperature properties and it may well be in this area that the unique thermal histories associated with atomization could play an important role. The high values of nucleation undercooling which are experienced by fine metal droplets due to the effective reductions in heterogeneous nucleation resulting from the subdivision of the melt (see [3]) may be exploited to best effect by the use of alloys displaying partition coefficients greater than one (i.e. peritectic systems). In such alloys the initial rapid cooling rates experienced by the droplets can lead to the prevention of nucleation of the complex intermetallic unit cell until the temperature regime is entered in which the more simple f c c aluminium may nucleate. Growth of this phase will take place with negative partitioning, leading to a cellular structure with solute-rich cells and solute-lean intercellular regions [14]. Such structures, it is thought, may well provide the best starting microstructures for the development of alloys which will best utilize the unique processing parameters associated with atomization. This work is currently being undertaken and it is hoped to present the results in future publications.

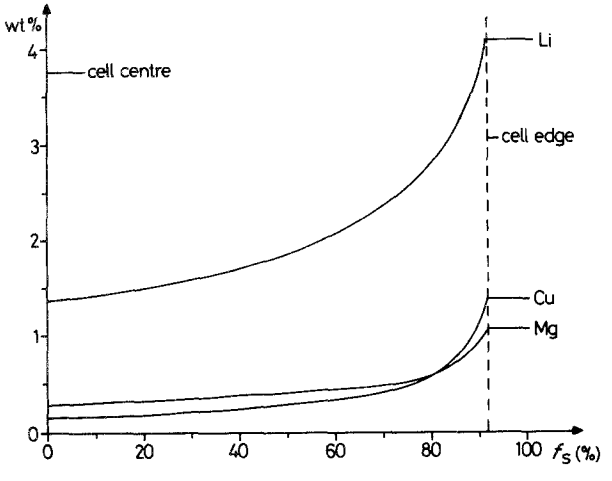

Figure 11 Calculated composition profile (Scheil analysis) across a cell. For discussion see text.

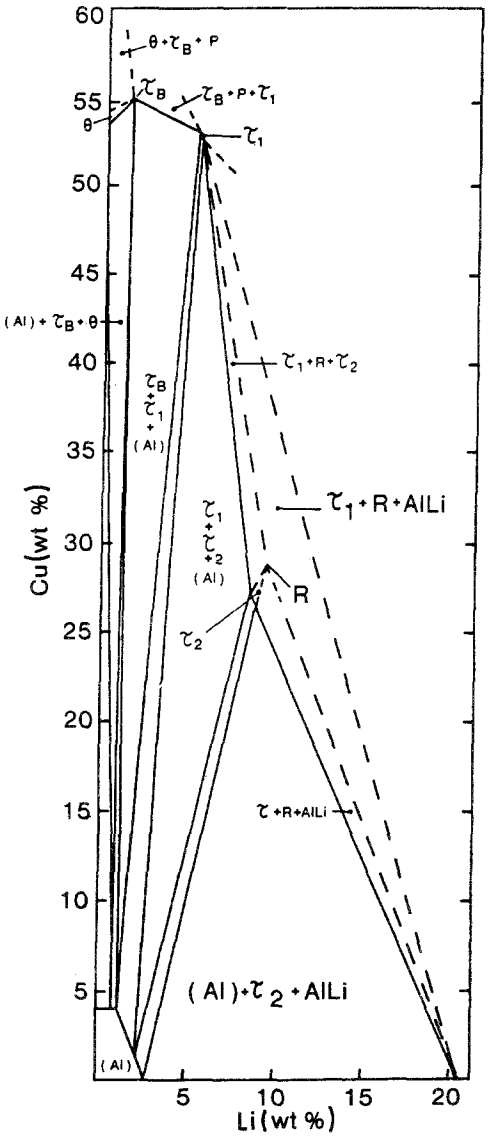

Figure 12 Isothermal section (500° C) of Al–Cu–Li ternary phase diagram.

5. Conclusion

The results presented in this paper relate to the development of solidification microstructures in small metal droplets produced by inert gas atomization. For eutectic type alloys, of which current low density alloys are an example, microcellular solidification microstructures are produced and the results presented here show that equilibrium solute partitioning takes place for the particle size range likely to be of most interest (10 to 20 μm). Consideration of the dependence of heat transfer coefficient with particle size indicates that the achievement of enhanced solid solubilities by atomization in powders of this size is unlikely and utilization of the high degree of nucleation undercooling associated with melt subdivisions (i.e. atomization) may well provide the optimum alloy properties. Such alloys will probably also contain solute elements which exhibit partition coefficients greater than one and have complex equilibrium intermetallic phases which are likely to prove difficult to nucleate thus allowing the development of a cellular solidification microstructure with solute-rich cell centres. This microstructure may well respond to subsequent processing and heat treatment to provide an alloy with enhanced mechanical properties.

Acknowledgements

The authors would like to thank Professor A. P. Miodownik for the provision of laboratory facilities and for many stimulating discussions. Ms J. Mullervy is acknowledged for the preparation of the ultramicrotomed specimens and Dr P. M. Budd is thanked for the help with the collection and processing of the EELS data. G. von Bradsky wishes to thank the S. E. R. C. for the provision of a maintenance grant during the course of this work. The authors also wish to thank Dr G. Marshall for helpful discussions and Alcan International Ltd (Banbury) for the supply of material used in this investigation.

References

1. M. H. TOSTEN, A. K. VASUDÉVAN and P. R. HOWELL, Proceedings, Third International Al–Li Conference, University of Oxford, edited by C. Baker, P. J. Gregson, S. J. Harris and G. J. Peel (Institute of Metals, 1986) p. 483.
2. J. C. HUANG and A. J. ARDELL, *ibid.*, p. 455.
3. T. W. CLYNE, R. A. RICKS and P. J. GOODHEW *Int. J. Rapid Solid.* **1** (1984) 59.
4. T. W. CLYNE, R. A. RICKS and P. J. GOODHEW, *ibid.* **1** (1984) 85.
5. R. A. RICKS and T. W. CLYNE, *J. Mater. Sci. Lett.* **4** (1985) 814.
6. T. W. CLYNE, R. A. RICKS and P. J. GOODHEW, Proceedings, 5th Conference on Rapidly Quenched Metals (R.Q.5) Wurzburg, Germany, 1984 edited by S. Steeb and H. Warliment, (North Holland Physics Publishing, Amsterdam) p. 903.
7. P. K. DOMALAVAGE, N. J. GRANT and Y. GEFEN, *Met. Trans A* **14A** (1983) 1599.
8. R. A. RICKS, Proceedings, Institute of Physics E.M.A.G. Conference, Newcastle, edited by G. Tatlock (1985) p. 493.
9. R. A. RICKS, P. M. BUDD, P. J. GOODHEW, U. L. KOHLER and T. W. CLYNE, Proceedings Third International Al–Li Conference, University of Oxford, edited by C. Baker, P. J. Gregson, S. J. Harris and C. J. Peel (Institute of Metals, 1986) p. 97.
10. H. M. CHAN and D. B. WILLIAMS, *Phil. Mag. B* **52** (1985) 1019.
11. M. C. FLEMING, "Solidification Processing" (McGraw Hill, New York, 1974) p. 34 ff.
12. G. J. MARSHALL, Proceedings, Aluminium Technology '86 Conference, London (1986) Institute of Metals paper 82.
13. R. A. RICKS, N. J. E. ADKINS and T. W. CLYNE, Proceedings, Institute of Metals Powder Metallurgy Group Meeting (1985) Eastbourne, paper No. 8.
14. R. A. RICKS and N. J. E. ADKINS, Proceedings, Aluminium Technology '86 Conference, London (1986), Institute of Metals, paper 80. 11.

Received 3 June
and accepted 18 August 1986